Colloids and Surfaces A: Physicochemical and Engineering Aspects 684 (2024) 133165

Contents lists available at ScienceDirect

Colloids and Surfaces A: Physicochemical and Engineering Aspects

journal homepage: www.elsevier.com/locate/colsurfa

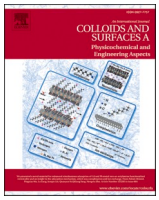

Molecular dynamics simulation of oil displacement using surfactant in a nano-silica pore

Wei Yong [a,b], Zhijie Wei [a,b], Yingfang Zhou [c,*]

[a] National Key Laboratory of Offshore Oil and Gas Exploitation, Beijing 100028, China
[b] CNOOC Research Institute Co. Ltd., Beijing 100028, China
[c] School of Engineering, University of Aberdeen, Aberdeen, UK

HIGHLIGHTS

- Oil water interfacial thickness increases significantly after adding surfactant.
- Oil droplet contact angle increases with surfactant addition.
- Oil droplet deformation and displacement speed have a positive relation with the static contact angle.
- Surfactant can significantly increase oil displacement velocity.

GRAPHICAL ABSTRACT

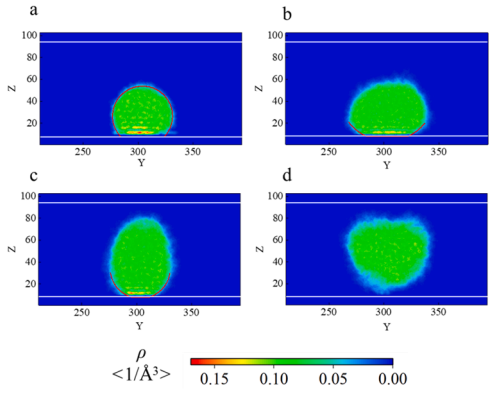

ARTICLE INFO

Keywords:
Interfacial tension
Contact angle
Surfactant flooding
Silica nanopore
Molecular dynamics simulation

ABSTRACT

Molecular Dynamics (MD) simulations of oil droplet displacement have been performed using pressure driven surfactant flooding at a typical reservoir condition (T = 330 K and P = 20 MPa). The behavior of the micellization of surfactant molecules has been validated. A micelle with a radius of 22.85 Å is formed by 60 anionic sodium dodecyl benzenesulfonate (SDBS) surfactant molecules in aqueous solution. Surfactant additions result in significant reduction of interfacial tension (IFT) for oil/water system and such reduction is dependent on surfactant surface concentration. The microscopic mechanism of IFT reduction is described. Interfacial thickness increases from 3.5 Å to 22.5 Å at T = 300 K and$P$ = 1 atm after surfactant molecules are adsorbed at oil/water interface, indicating high miscibility of two phases and thus results in interfacial tension reduction; the calculated interface formation energy of a single surfactant molecule is −145.7 Kcal/mol, which means the additions of surfactant would lead to the decrease of system energy and thus a more steady system. For surfactant flooding simulation, oil droplet static contact angle increases with surfactant additions. The larger the static contact angle of oil droplet, the stronger the drop deformation and the higher the displacement speed. Limited deformation is observed as oil droplet detaches from the solid substrate. Compared with water flooding, surfactant additions can significantly increase oil displacement speed by up to 80 %.

* Corresponding author.
E-mail address: yingfang.zhou@abdn.ac.uk (Y. Zhou).

https://doi.org/10.1016/j.colsurfa.2024.133165
Received 4 September 2023; Received in revised form 25 December 2023; Accepted 4 January 2024
Available online 11 January 2024

1. Introduction

From a macroscopic perspective, surfactant molecules adsorb on oil–water interface and form a monolayer [45]. This behavior enhances the interfacial interactions (surfactant hydrophilic headgroup–water interaction and surfactant hydrophobic tails–oil interaction) and significantly reduces the interfacial tension (IFT) between oil and water [12,17]. The reduction of IFT further results in change in wettability (as quantified by contact angle) at oil/water/rock interface, influencing capillary pressure and capillary number. These factors play an important role in the EOR process [2,46]. However, the microscopic mechanism, such as water/oil interfacial behavior, the oil droplets aggregation, displacement and transport in nanopores under surfactant flooding, is still lack of proper investigation.

Surfactant flooding has shown promise as a potential enhanced hydrocarbon recovery technique in tight formations due to its efficiency in reducing the IFT between oil and water [20,22,34]. Experimental investigation on the displacement process of using surfactant to extract hydrocarbon in tight formation is very challenging due to its length scale, and recently Molecular Dynamics (MD) simulations have been proposed to study the microscopic absorption and transport mechanism of oil molecules in nanopores [10,35,36,38]. These authors have performed prominent work that well complements experimentation. For MD work relating to surfactants, Gan et al. [11] studied the effect of ionic surfactants on the wettability of coal. The structure dynamics of surfactant micelles has been discussed in [26], and Xu et al. [39] has explained how the surfactant headgroups affects the oil/water interface. Tang et al. [36] studied the detachment of the crude oil aggregate in silica nanochannel under surfactant flooding using MD simulations and they pointed out that the detachment of oil molecules started from the rear bottom of the oil aggregate. However, the microscopic mechanism of IFT reduction with surfactant additions is still not clear and how its resulting wettability alteration controls oil transport behaviors in nano silica pores needs to be further investigated.

In this work, MD simulations of interactions between oil/water/surfactant molecules in a nano-silica pore at a typical oil reservoir condition (T = 330 K and$P$ = 20 MPa) have been performed to investigate the microscopic mechanism of oil/water IFT reduction using surfactant molecules, and the effect of surfactant molecules on oil droplet transport in nanopore. This article is organized as follows: the model system, geometry and the simulation approach as well as the force field parameters are summarized first. Then results on surfactant micelles in aqueous solution and IFT for oil/water/surfactant system are presented. The deformation and transport of oil droplet under an external driving force – mimicking the constant pressure gradient – in a nano silica pore is discussed. The paper is closed with main conclusion and future work. For the field to which it is applied, the findings of the present work can help to design the molecular architecture of surfactant for the purpose of optimizing the oil/water performance, and to determine the surfactant usage dose and solution concentration in surfactant flooding.

2. Molecular dynamics simulation setups

2.1. Nanoscale slit pore and fluids

First, the silica lattice of α-SiO_2 is derived from the database of the Materials Studio software [1]. Then it was expanded into α-quartz silica supercell with orthorhombic dimensions (xyz) of 24.6 × 595 × 102 Å^3. Given the size range of nanopores in reservoir [9], the middle part of the silica supercell is removed and thus a slit pore with a height of 86.6 Å along the y axis is constructed, see Fig. 1. The silica surface is further hydroxylated by –OH group with a density of 9.6 nm^2, in line with previous MD work [41] and the result of crystal chemistry calculations [18].

Surfactant majorly includes cationic and anionic surfactants. Tang et al. [36] and Pan et al. [27] presented excellent work on the effect of anionic and cationic surfactant on IFT and contact angle numerically and experimentally, respectively. It is found that as compared to the headgroup (for example the $-N(CH_3)_3^+$) in cationic surfactant, the group (like $-SO_3^-$) in anionic surfactant has a stronger H bond interaction with surrounding water molecules. The stronger interaction induced a quicker surfactant on oil aggregate surface and hence accelerates the detachment of oil drop. Both cationic and anionic surfactant have distinct effects on decreasing IFT while the anionic has a higher oil-driven efficiency.

In the present work, the surfactant molecule selected is anionic sodium dodecyl benzenesulfonate (SDBS, $C_{18}H_{29}NaO_3S$), which is a common surfactant used in petroleum industry for oil recovery [24], and it has been widely applied in MD studies to investigate the surfactant interactions with the oil molecular aggregate [19,39]. The oil is represented by dodecane, $C_{12}H_{26}$ [3], and the three-stie water model (H_2O) is used in this study.

2.2. Molecular dynamics simulation

Our simulation system consists of water, oil ($C_{12}H_{26}$), surfactant (SDBS, $C_{18}H_{29}NaO_3S$) and silica nano slit pore. In all MD simulations, the water, oil, surfactant, and silica are all described by the full-atom force field – the polymer consistent force field (PCFF) [33]. It is known that the PCFF has been validated to accurately describe structural and thermodynamic properties of oil component and organic compounds [4,36,39,40]. For example, in the work of [39], they reported a 7 % difference in their MD results on oil/water interfacial tension using PCFF with experimental data.

The total potential energy of the system includes bonded terms and nonbonded interaction terms (Coulombic and Lennard–Jones functions). The functional forms can be expressed as following:

$$E_{total} = E_{bonds} + E_{angles} + E_{torsions} + E_{non-bonded} \quad (1)$$

$$E_{non-bonded} = \sum_{i}^{N}\sum_{j>i}^{N}\left(\varepsilon_{ij}\left[2\left(\frac{\sigma_{ij}}{r_{ij}}\right)^{9} - 3\left(\frac{\sigma_{ij}}{r_{ij}}\right)^{6}\right] + \frac{q^i q^j}{4\pi\varepsilon_0 r_{ij}}\right) \quad (2)$$

the $\varepsilon_{ij}$and σ_{ij}represent the strength and the length scale of the LJ interaction respectively; q^i and q^j are the charges of sites i and j, and ε_0 the dielectric permittivity of the vacuum. Each atom type α has been given its own size σ_α and strength ε_α. The cross interaction LJ – 9–6 parameters for unlike pair atoms ($\alpha$and β) are calculated from a 6th order combination law [37]: $\sigma_{\alpha\beta} = \left(\frac{\sigma_\alpha{}^6 + \sigma_\beta{}^6}{2}\right)^{1/6}$ and $\varepsilon_{\alpha\beta} = 2\sqrt{\varepsilon_\alpha\varepsilon_\beta}\left(\frac{\sigma_\alpha{}^3\sigma_\beta{}^3}{\sigma_\alpha{}^6+\sigma_\beta{}^6}\right)$. The LJ – 9–6 interactions have a cut-off distance of 12 Å. The particle-particle particle-mesh (PPPM) algorithm [6] with a convergence parameter of 10^{-4} is used to treat the long-range (beyond 12 Å cut-off) electrostatic interactions. The complete set (of parameters) is given in supplementary document. The full chemical structure of water, oil and surfactant molecules used in this paper is presented in Fig. 2.

Solid atoms are fixed at their initial positions due to a negligible thermal motion impact on the dynamics of the fluid molecules [30,32,42]. All MD simulations were performed using the open-source molecular dynamic simulation code LAMMPS [28] with a periodic boundary condition. A time step of 1 fs [36] is used in this work.

3. Results and discussion

The structure of micelle formed by surfactant molecules in aqueous solution and the interfacial tenson of oil/water and oil/water/surfactant system were investigated first using MD simulations.

3.1. Surfactant micelles in aqueous solution

60 SDBS molecules are placed in the center of a cubic domain con-

Fig. 1. Schematic illustration of the nano slit pore. The pore width equals to 86.6 Å with dimensions x and y of 24.6 and 595 Å.

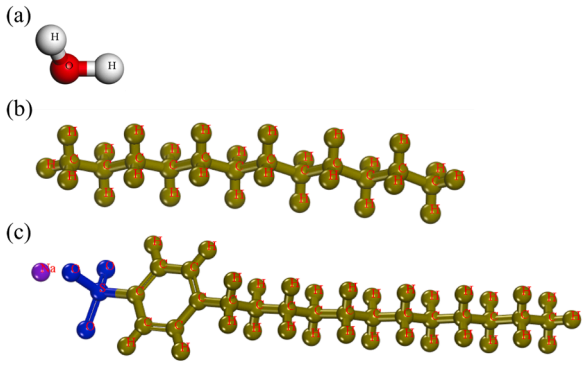

Fig. 2. Full chemical structure and the atom types of (a) water, (b) dodecane and (c) SDBS. For SDBS molecule, the head group (SO_3^-) is marked as blue and the hydrocarbon chain is olive.

taining 14275 water molecules with 80 × 80 × 80 Å. The number of 60 is a reasonable mean aggregation number (the number of micelle molecules that form an aggregate) for SDBS micelles after an experimental study [5] and also matches the number used in the recent simulations [26]. The system is first evolved in a 1 ns NVT ensemble at a fixed T = 300 K and then in a 4 ns NPT ensemble at T = 300 K and$P$ = 1 atm. In the NPT evolution, the box length allows to get changed in all three Cartesian coordinate directions. In the last 1 ns, data are collected and processed to generate results under NPT. Finally, the equilibrium box size is 76 × 76 × 76 Å, and the water density of the system is 0.972 ± 0.03 g cm^{-3}, close to NIST webbook density of 0.997 g cm^{-3} at T = 300 K and$P$ = 1 atm [31].

A snapshot of the equilibrium water/surfactant system is shown in Fig. 3 **(a)**. A SDBS micelle (an aggregate formed by 60 surfactant molecules) with a sphere shape is clearly seen in the bulk aqueous phase. The hydrocarbon chains of surfactant molecules present hydrophobic property and form the core of the aggregate. The head groups are hydrophilic and thus are in contact with surrounded water molecules. This qualitative behavior of the aggregate agrees well with the observations in the previous studies of micellization of SDBS surfactant molecules process in aqueous solution [26,36].

We now quantitatively analyze the SDBS micelle structure in terms of the probability distribution of the distance of selected atoms (sulfur S and carbon C) from the center of mass of the micelle, r_{com}. In Fig. 3 **(b)**, our simulated results are in good agreement with MD work of Palazzesi et al. [26]: "the carbon atoms density (including all of the carbon atoms

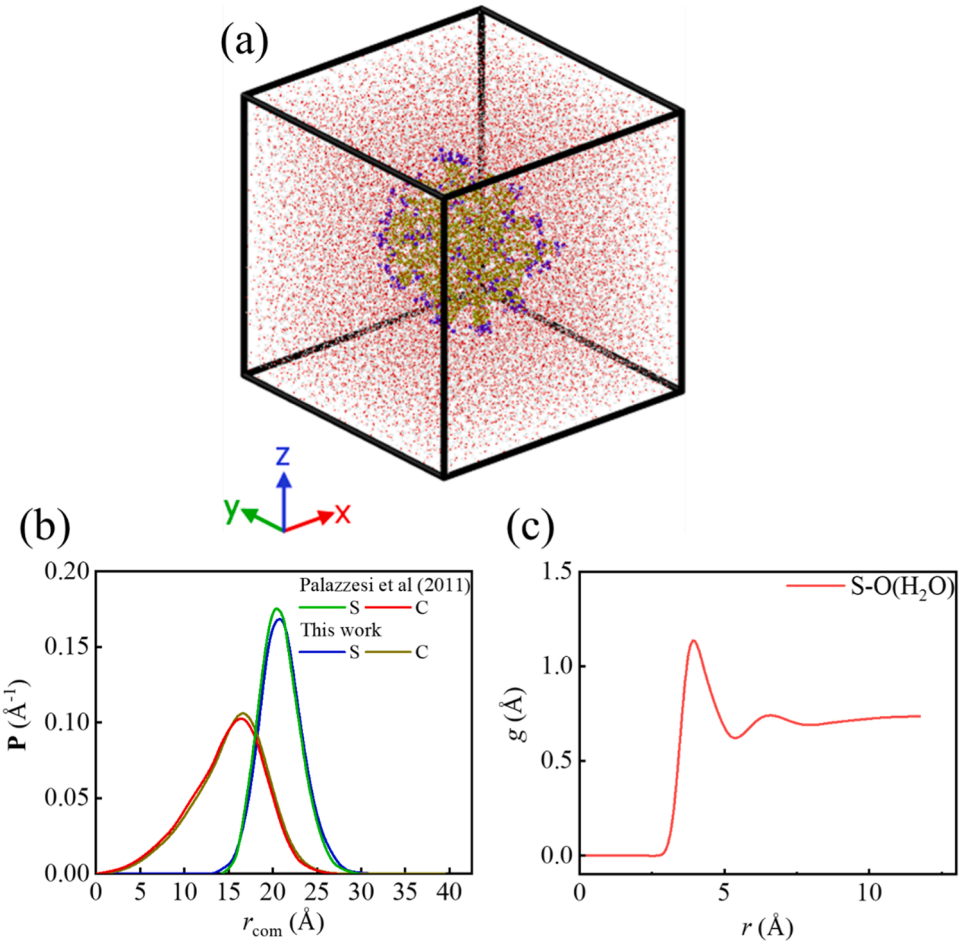

Fig. 3. The structure of a SDBS micelle in aqueous phase. 60 SDBS molecules, T **= 300 K and**P = 1 atm. (a) A snapshot of the equilibrium shape of the SDBS micelle. (b) Probability distribution of the distance of atoms sulfur S (blue line) and atoms carbon C (olive line) from the center of mass of the micelle. Red and green line – MD simulations from [26]. (C) O (oxygen atoms in water molecules) radial distribution functions from S (sulfur atoms in surfactant molecules).

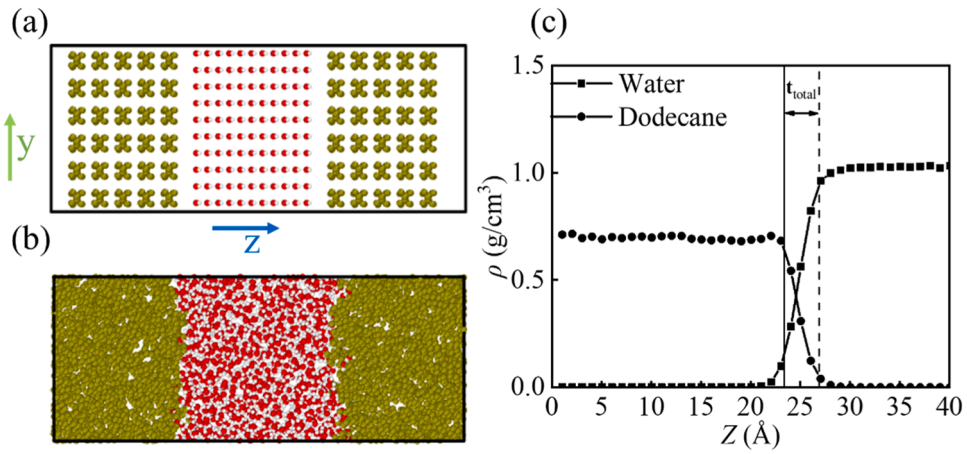

Fig. 4. Configuration of oil/water system simulation at $T = 300$ K and $P = 1$ atm. A schematic of initial (a) and equilibrium (b) dodecane/water system. (c) The average density profiles of water and dodecane along Z axis normal to the plane of the interface. Error bars are less than the symbol size. Vertical solid and dash lines (defined by the "90–90″ criterion) are two distinctions between which is defined as oil/water interfacial thickness, t_{total}.

in SDBS molecules) rapidly decreases between 16 and 22 Å for SDBS micelle; the sulfur atoms density rapidly decreases between 21 and 25 Å". As shown in this figure, the paraffinic (alkanes) radius r_{C-com} reads 16.5 Å, and the distance of sulfur atoms of the head group from the micelle center of mass, r_{S-com}, is 20.5 Å. The simulated results agree with the experimental work by [15], where authors reported a paraffinic radius of 16.7 Å using the small angle X-ray scattering (SAXS) of sodium dodecyl sulfate (SDS) micelles. The SDS micelles have an almost identical (difference is within 5 %) carbon atoms and sulfur atoms distribution with SDBS micelles [26].

The radius of SDBS micelle is further investigated. The radius of the micelle has been defined "as the average distance between the sulfur atoms of the head group from the micelle center of mass plus the distance between the first peak of the water oxygen radial distribution function from the sulfur atoms ($r_{S-o(H_2O)}$) minus the radius of water" [26]. Our results show$r_{S-o(H_2O)}$, see Fig. 3 **(c)**, is 3.75 Å, in line with Palazzesi et al.'s (2011) result of 3.43 Å. The final radius of SDBS micelles is 22.85 Å, close to pervious MD result of 22.42 Å [26] and experimental result of 22.3 Å [15].

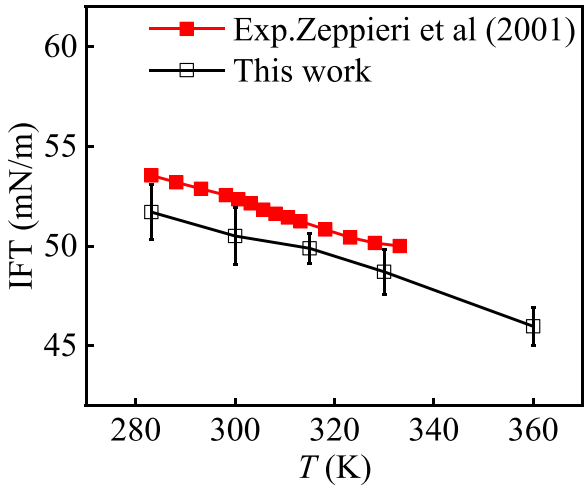

Fig. 5. Interfacial tension of the dodecane-water interface as a function of temperature at $P = 1$ atm. Our simulation data compared to experimental data from the literature as indicated.

3.2. Interfacial tension between oil and water

3.2.1. Oil/water system without surfactant

A symmetric two-phase system with 32 × 32 Å in X and Y direction consisting of dodecane and water is constructed as in Fig. 4 **(a)**. A 30 Å thick slab of liquid water (1024 water molecules based on 0.997 g cm^{-3} for water at $T = 300$ K$P = 1$ atm) is placed at the middle of the system. The system is under this T and P condition for comparison with available simulation and experimental data. At two sides of the water phase are two oil slabs, with each length of 22.3 Å containing 60 dodecane molecules (0.744 g cm^{-3} for dodecane at $T = 300$ K$P = 1$ atm from NIST webbook data [31]). A 1 ns NVT simulation at 300 K as a pretreatment and an NPT simulation for 6 ns at $T = 300$ K and $P = 1$ atm are sequentially carried out. Fig. 4 **(b)** shows an equilibrium snapshot of oil/water system. Data in last 4 ns is collected and used in the calculations related to interfacial properties.

The equilibrium average density profiles of water and oil along Z axis normal to the plane of the interface is shown in Fig. 4 **(c)**. Then the average density is calculated over 200 independent realizations. This allows to determine the interfacial thickness of oil/water system. The interfacial thickness is an important parameter relating to the interfacial tension and has been defined as "the distance between two positions where the densities of oil and water are 90 % of their own bulk densities [16]", i.e., the "90–90″ criterion. The vertical solid line and dash line are used to represent the "90 % water bulk density position" and the "90 % dodecane bulk density position" respectively, and the interfacial thickness, t_{total}, of the oil/water system is 3.5 ± 0.08 Å. The findings are well in agreement with the value (3.38 Å) calculated from capillary wave theory [23].

As a planar interface with its normal in the Z-direction was created in a fully periodic domain, see Fig. 4 **(b)**, the interfacial tension γ was determined after equilibration according to [14].

$$\gamma = \frac{L_z}{2}\left[p_{zz} - \frac{1}{2}\left(p_{xx} + p_{yy}\right)\right] \tag{3}$$

where p_{xx}, p_{yy} and p_{zz} are the diagonal components of the pressure tensor and L_z the domain length in the Z-direction. The pressure tensor $p_{\alpha\beta}$ is given by the virial expression [14].

$$p_{\alpha\beta}V = \left\langle \sum_{i=1}^{N} m_i \mathrm{v}_{\alpha,i}\mathrm{v}_{\beta,i} + \sum_{i=1}^{N-1}\sum_{j>1}^{N} r_{\alpha,ij} f_{\beta,ij} \right\rangle \tag{4}$$

with V the volume of the simulation domain, N the total number of atoms, $\mathrm{v}_{\alpha,i}$ the velocity component in the α direction of atom i and $r_{\alpha,ij}$

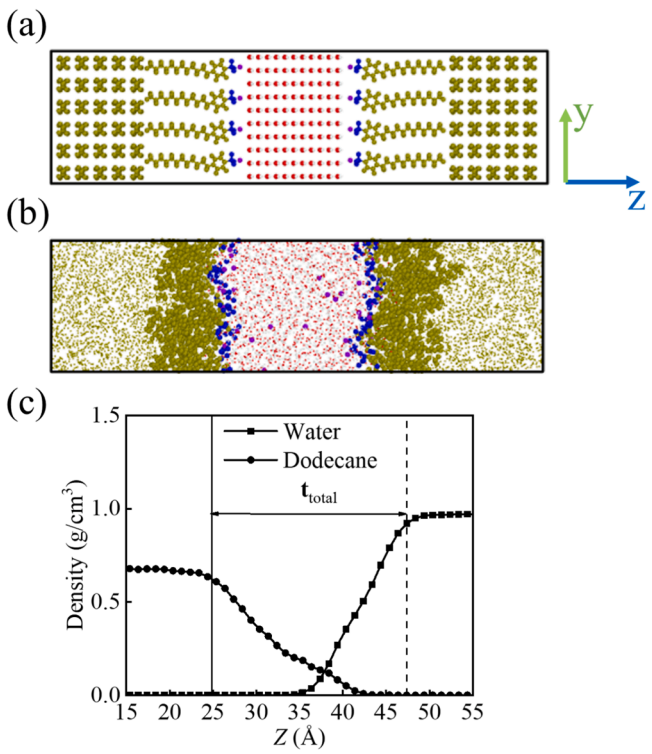

Fig. 6. A schematic of initial (a) and equilibrium (b) dodecane/water/SDBS system at T = 300 K and$P$ = 1 atm. Sizes for dodecane and water molecules are adjusted for clarity. (c) The density profiles of water and dodecane along Z axis normal to the plane of the interface. Vertical solid and dash lines are two distinctions between which is defined as oil/water interfacial thickness, t_{total}.

and $f_{\alpha,ij}$ the α component of vectors $\mathbf{r_{ij}}$ and $\mathbf{f_{ij}}$ respectively. The angled brackets stand for ensemble averaging.

Our simulated interfacial tension $\gamma = 50.5 \pm 1.42$ mN/m at $T = 300$ K and $P = 1$ atm matches well with experimental measurement of IFT of dodecane/water system (52.34 mN/m) at the same $T$and$P$condition [44]. However, the simulated IFT is slightly lower than the reported 56.23 mN/m in the experimental work part in [39]. The uncertainty in interfacial tension is determined by calculating its standard deviation from 10 time intervals.

The temperature sensitivity with respect to IFT is further investigated by varying the T from 283 K to 360 K. We discuss about the liquid water in this paper and thus the T cannot exceed 373.15 K at 1 atm. In Fig. 5 the simulated results of IFT versus T are compared to experimental data. Our simulations follow the overall trend as found in previous studies: a decrease in interfacial tension with increasing temperature until the temperature reaches a value of the order of 360 K where interfacial tension has reduced by about 11 % as compared to the value of the order of 283 K. The simulated interfacial tension is systematically on the lower side compared to measured data (the difference is within 5 %) [44]. Possible reasons for theses deviations could be (from the simulation perspective): the size effects and the effect of time step. For experimental factors: the difficulty in the measurement of IFT (including the difficulty in keeping the experimental setup clean and the fluids might get chemically modified after chemical interaction with the experimental setup) would also contribute to the experimental uncertainty [14]. The results in Fig. 5 provide a baseline data set and starting point for studying the effects of surfactant on oil/water interfacial tension.

3.2.2. Oil/water/surfactant system

Based on the initial configuration of oil/water system as shown in Fig. 4 **(a)**, two slabs of symmetric surfactant molecules are added in between the oil phase and water phase. Each surfactant slab contains 16 SDBS molecules with their headgroups organized in a 4×4 square lattice in xy plane [39] and pointing at the middle water phase, see Fig. 6 **(a)**. This gives the surface area per molecule of 64 Å^{-2}, following with the experimentally observed value for adsorption at air/water interface at their critical micelle concentration (CMC) [29]. In this study, the surfactant surface concentration Γ is used to describe the interfacial properties.

The same procedure (including the data post-processing for IFT) is repeated for oil/water/surfactant system as in oil/water system. The simulated γ for oil/water/surfactant equals to 8.35 ± 0.68 mN/m, that is an 83 % decrease from 50.5 ± 1.42 mN/m for oil/water at $T = 300$ K and $P = 1$ atm. In experimental work [39], they reported a value of 8.03 mN/m for dodecane/water/SBDS system measured via the spinning drop technique. Fig. 6 **(b)** shows an equilibrium schematic of oil/-water/surfactant system. With surfactant additions, the surfactants self-assemble into monolayer on the oil/water interface. The hydrophobic hydrocarbon chain inserts into oil phase and the hydrophilic headgroup is in contact with water phase. As described in the *Introduction* section, the monolayer enhances the interfacial interactions (surfactant hydrophilic headgroup – water interaction and surfactant hydrophobic tails – oil interaction), and thus would decrease the surface energy of oil and water phase and thus IFT.

IFT is closely related to interfacial thickness and interface formation energy (IFE) [7,16], which is investigated very limited by experimental studies. We now turn to the mechanism of these two factors on the IFT reduction from a microscopic perspective, via MD simulations. Fig. 6 **(c)** shows the density profiles of water and oil along Z axis normal to the plane of the interface for the equilibrium oil/water/surfactant system. It is seen that the calculated interfacial thickness (based on the "90–90″ criterion) is 22.5 ± 0.16 Å, that is a distinct increase from 3.5 Å for the oil/water system where surfactant is in absence. One reason for the increase in oil/water interfacial thickness is: the hydrophilic headgroups and the hydrophobic tails in the surfactant monolayer insert into the water and oil phase after surfactant/water and surfactant/oil attractions; as a result, the permeation of water and oil in the self-assembly surfactant membrane leads to the increase of the water interfacial thickness and oil interfacial thickness, respectively, and thus the total oil/water interfacial thickness t_{total} increases. Large interfacial thickness usually indicates high miscibility of oil/water phases [39], and the oil/water interfacial tension decreases after adding surfactant.

The energetic stability influences interfacial property [16]. The interface formation energy of single surfactant molecule is expressed as

$$\mathrm{IFE} = \frac{E_{total} - \left(n \times E_{surfactant,single} + E_{\mathrm{dodecane-water}}\right)}{n} \tag{5}$$

where E_{total}, $E_{surfactant,single}$, and $E_{\mathrm{dodecane-water}}$ denote the potential energies of whole system, the single surfactant molecule that is calculated from a separate MD simulation in vacuum at the same temperature, and a bare dodecane-water system. The variable n is the number of surfactant molecules. The IFE is generally negative. It means the additions of surfactant would lead to the decrease of system energy and thus the system would be more stable [39]. IFE is also a measure of the average intermolecular interaction per surfactant molecule as the result of the addition of one surfactant molecule into the dodecane-water interface. The larger IFE means a stronger interaction between surfactant/dodecane and surfactant/water. The strong intermolecular interaction means high capability of decreasing interfacial tension [16]. The calculated IFE of a single surfactant molecule is − 145.7 Kcal/mol in this study, between the value of 73.9 and of 264.72 Kcal/mol reported by Xu et al. [39] and Jang et al. [16].

The number of surfactant molecules - that are placed on oil/water interface - is varied to study the effect of surfactant surface concentration (Γ) on IFT. The number of surfactant molecules has been adjusted

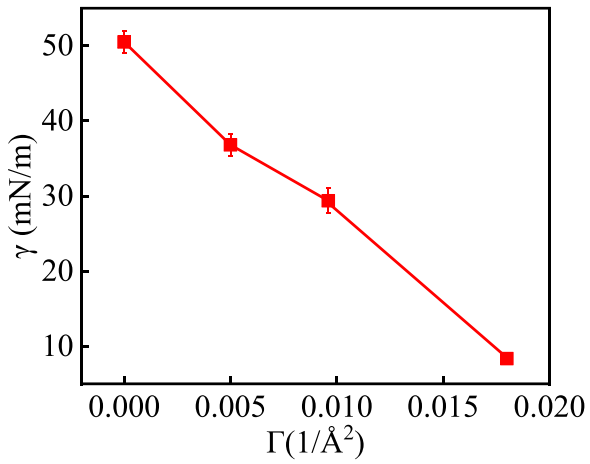

Fig. 7. Interfacial tension of the dodecane/water/surfactant system as a function of surfactant surface concentration (Γ) at T = 300 K and P = 1 atm.

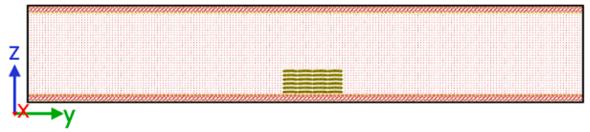

Fig. 8. The initial configuration for water flooding system. Water molecules sizes have been adjusted for clarity. T = 330 K and P = 20 MPa (a typical reservoir condition). The pore width equals to 86.6 Å.

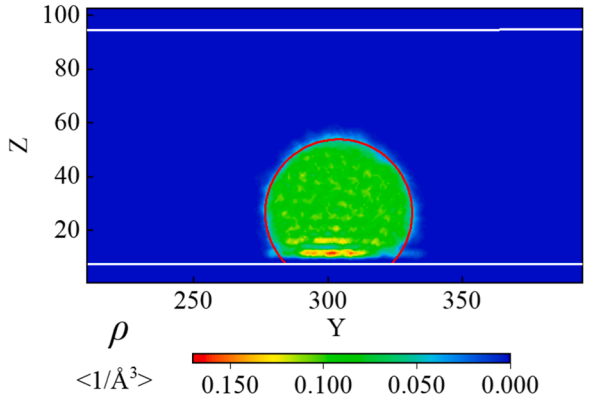

Fig. 9. Equilibrated oil droplet shape as a result of a time averaging over 2 ns in EMD water flooding simulation. T **= 330 K and** P = 18.5 ± 0.6 MPa. The red curve is the best fit of a circular arc to the interface. The white line at the bottom is at the highest location of atoms constituting the silica surface.

from 8 to 32 to generate four oil/water/surfactant systems with different surfactant surface concentration from 0.005 to 0.018/Å^2. The corresponding IFT with Γ is shown in Fig. 7. IFT has a significant reduction (about 77 %) from 36.8 ± 1.46 mN/m to 8.35 ± 0.68 mN/m at T = 300 K and P = 1 atm, which agrees well with the trend observed previously by Nguyen et al., [25]. Our simulated results provide a proper data support for surfactant related oil/water interface studies and also for experimental validation.

3.3. Water flooding

The initial configuration for water flooding is shown in Fig. 8. 120 dodecane molecules are placed in the center of the bottom silica surface, and 37520 water molecules are added in pore to form a typical reservoir condition, T = 330 K and P = 20 MPa [41]. A 4 ns equilibrium MD

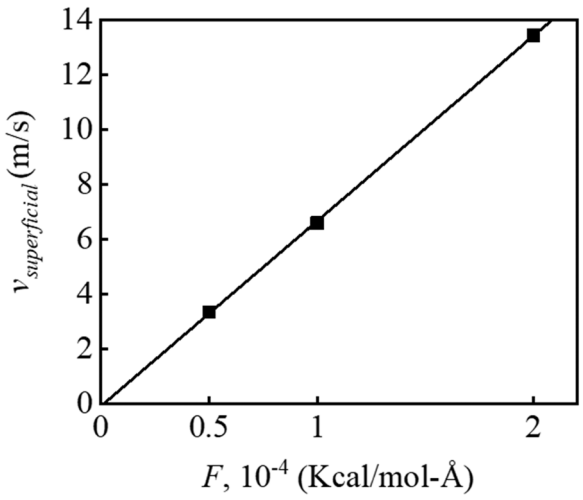

Fig. 10. Water average superficial velocities versus various F. T **= 330 K and** P = 18.5 ± 0.6 MPa. Error bars are less than symbol size.

(EMD) simulation is first conducted in a NVT ensemble at T = 330 K. Data in the latter 2 ns are collected for static contact angle estimation. The pressure after equilibrium is 18.5 ± 0.6 MPa. The equilibrated oil droplet is shown via the averaged density contour as in Fig. 9. The angle with which the red arc intersects with the top silica surface is estimate for static contact angle. The estimated contact angle is 132.39 ± 3.4°. The uncertainty is a result of the standard deviation calculation for contact angle over 5 different time intervals. For contact angle estimation, a detailed work on droplet size effect has been reported in our previous publication [42], in which the relations between contact angle and droplet size were well descripted by modified young's equation with line tension. In this paper, 120 dodecane molecules are used as oil drop for contact angle simulation, of which the number of molecules is comparable to reported oil droplet contact angle simulation work [20–22]. Besides, it requires to generate larger domain to consider increasing the size of drop, and thus it is computational expensive to run MD simulations. As a result, the size effect is ignored herein.

Then a 10 ns non-equilibrium MD (NEMD) simulation is followed. Temperature remains at T = 330 K. An external force F= 1.0 × 10^{-4} Kcal/mol-Å [13] is added to each water molecule to push water along the Y direction. For oil phase, 11.5 ×F is added on each dodecane molecule to form an identical force density with water phase. That approximately equals to 3 × 10^8 MPa/m. Such a large external force is necessary in MD simulation as previously discussed in our work [43]. By varying the factors of F, the relationship between water average superficial velocities (volumetric flow rate divided by cross sectional area) and external force is studied. As shown in Fig. 10, water average superficial velocity is proportional to the external force F. This linearity helps to extrapolate the practical water flow (velocity) in realistic oil reservoir rock. The slope $\frac{v_{superficial}}{F} \propto W^2/\mu$, with W the width of pore and the μ the viscosity of the water.

The oil displacement speeds (v_s) by water flooding is presented by tracking the center of mass (COM) of oil droplet as a function of time, see Fig. 11. In left subfigure, these droplets center position exhibits linearity with time after external force is applied. The v_s is the slope of least squares fit with a straight line, as shown in right subfigure, which indicates that the oil displacement speed v_s is proportional to the external force F, or the pressure gradient.

3.4. Surfactant flooding

Surfactant molecules are added into after-equilibrium oil/water system to study the effect of surfactant flooding on oil droplet displacement. The number (N) of surfactant molecules are varied from

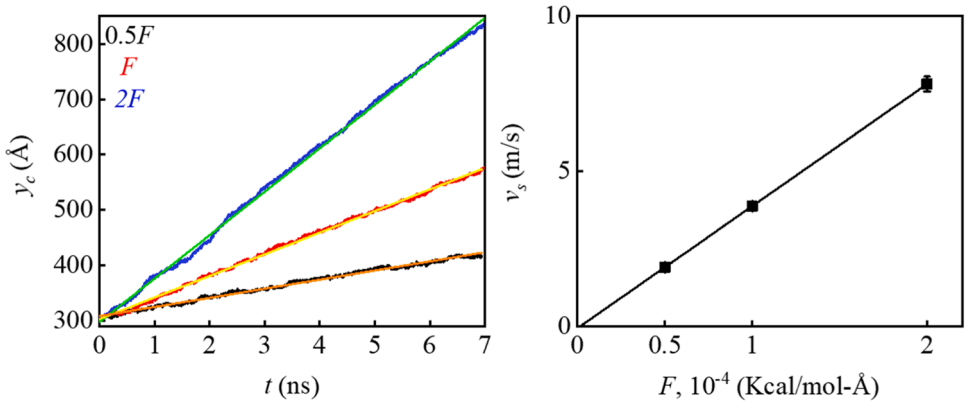

Fig. 11. Determining the displacement speeds (v_s). Left: center mass position of oil droplet (y_c) as a function of time for various *F*. The solid lines are best linear fits through the data points and the slope is the estimated average velocity v_s. Right: displacement speeds for various *F*. The straight line is best fits through the data points.

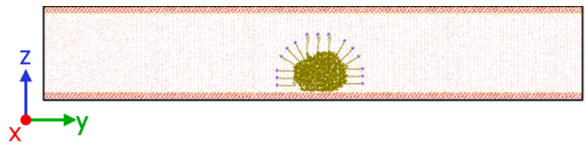

Fig. 12. The initial configuration for oil/water/surfactant system. Water molecules sizes have been adjusted for clarity. The width of pore is still 86.6 Å. The number of surfactant molecules N = 45. T = 330 K and P = 18.5 ± 0.6 MPa.

0 to 60. At the beginning, surfactant molecules are distributed around the equilibrated oil droplet (the equilibrated oil droplet can be seen in Fig. 9). An example of $N = 45$ is shown in Fig. 12. Similar with the simulation process in water flooding system, a 6 ns EMD simulation is first conducted, and the equilibrated oil/surfactant aggregate is shown in Fig. 13. An upward movement of oil droplet has been observed with surfactant molecules placed at oil/water interface and eventually lifts off the silica surface at $N = 60$. The strong interactions between oil/surfactants and water/surfactants due to the surfactant monolayer formed on oil/water interface results in oil droplet detachment and displacement (Sedghi 1998). The fitted contact angle for $N = 0$, 30, 45 and 60 (with corresponding Γ equals to 0, 0.004, 0.006 and 0.008 1/Å^2) are 132.39 ± 3.4°, 154 ± 3.7°, 161.93 ± 3.9° and 180° respectively. The surface surfactant concentration is calculated using the surface area of the oil droplet (excluding the base area) at equilibrium as in Fig. 13 **(a)**. In the fitting process, it is noted the oil/surfactant aggregate does not have a complete circular shape in Fig. 13 **b** and **c**, a section of circular fit through data near the interface is thus employed in the contact angle

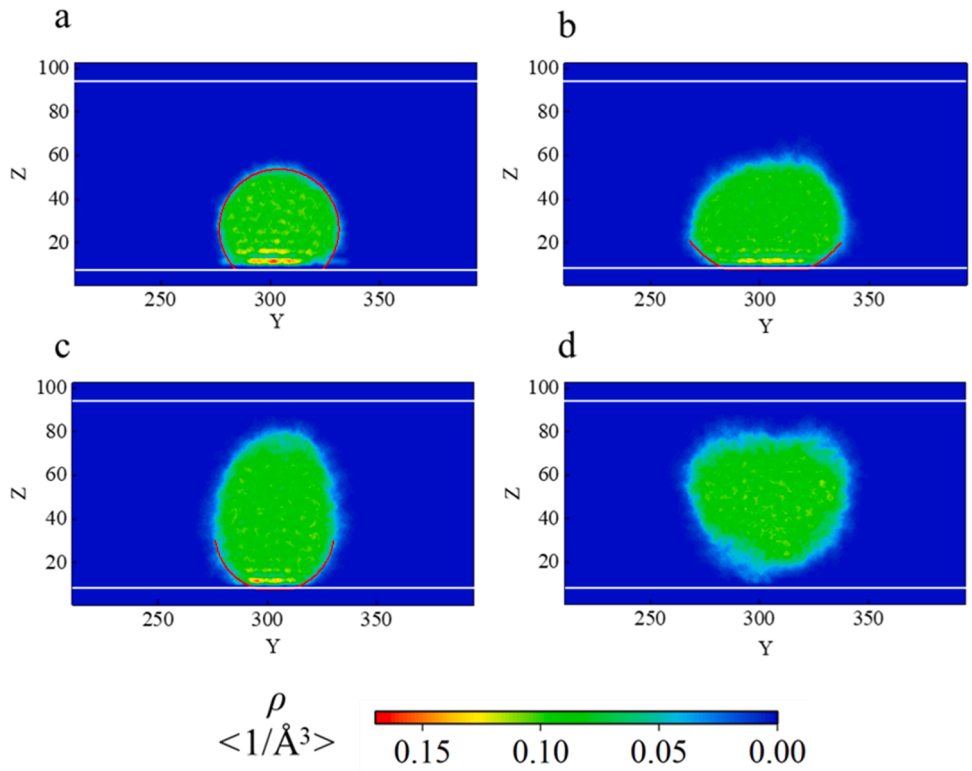

Fig. 13. Equilibrated oil/surfactant aggregate shape as a result of a time average over 4 ns in EMD oil/water/surfactant simulation. From a to d: the number of surfactant molecules N = 0, 30, 45, 60, with corresponding Γ equals to 0, 0.004, 0.006 and 0.008 1/Å^2, respectively.T = 330 K and$P$ = 18.5 ± 0.6 MPa. ρ is the oil/surfactant aggregate (oil and surfactant) density. The red curve is the best fit of a circular arc to the interface.

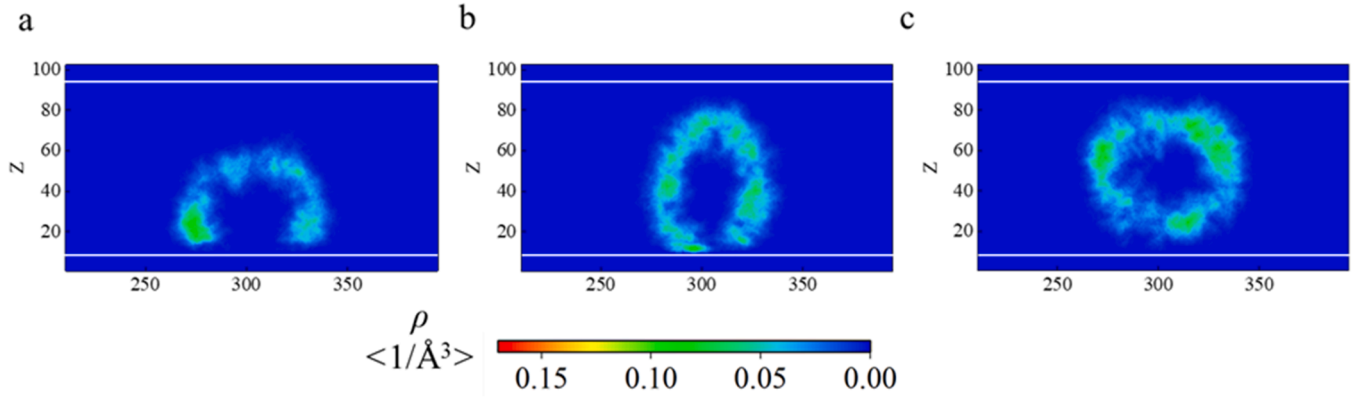

Fig. 14. Equilibrated surfactant density contours as a result of a time average over 4 ns in EMD oil/water/surfactant simulation. From a to c: the number of surfactant molecules N = 30, 45, 60.

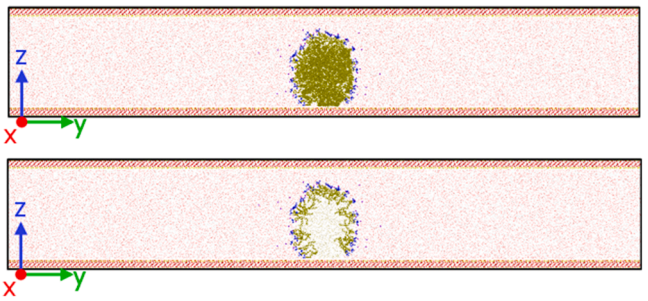

Fig. 15. Impression of surfactant molecules orientation after equilibrium for oil/water /surfactant EMD simulation at N = 45. T = 330 K and P = 18.5 ± 0.6 MPa. Water molecule sizes are adjusted for clarity. Top: oil/surfactant aggregate configuration. bottom: surfactant molecules configuration.

estimation. Besides, considering the layering effect [42], data located in 13 Å < Z < 22 Å and 13 Å < Z < 35 Å is used for circle fits. The surfactant density contour is shown in Fig. 14, where the surfactants are coating over the oil surface. The surfactants have a symmetric distribution around the centre of oil droplet. To further observe the surfactant molecules orientation at oil/water interface, a visual snapshot of the EMD simulation for oil/water/surfactant system after equilibrium is given, see Fig. 15. In this figure, surfactant molecules spread around oil phase and form a monolayer at oil/water interface with the hydrophobic alkyl chain (olive) inserting into oil phase and the hydrophilic headgroup (blue) immersing into water phase.

Then a 10 ns NEMD simulation for surfactant flooding is performed. External force distribution follows the same way as in water flooding system. The *F* keeps unchanged to form an identical pressure gradient as in water flooding simulation and a steady oil droplet shape is eventually reached (Water had *F*, both dodecane and surfactants have 11.5 *F*). Fig. 16 shows time-averaged (over 5 ns) droplet shapes where in the

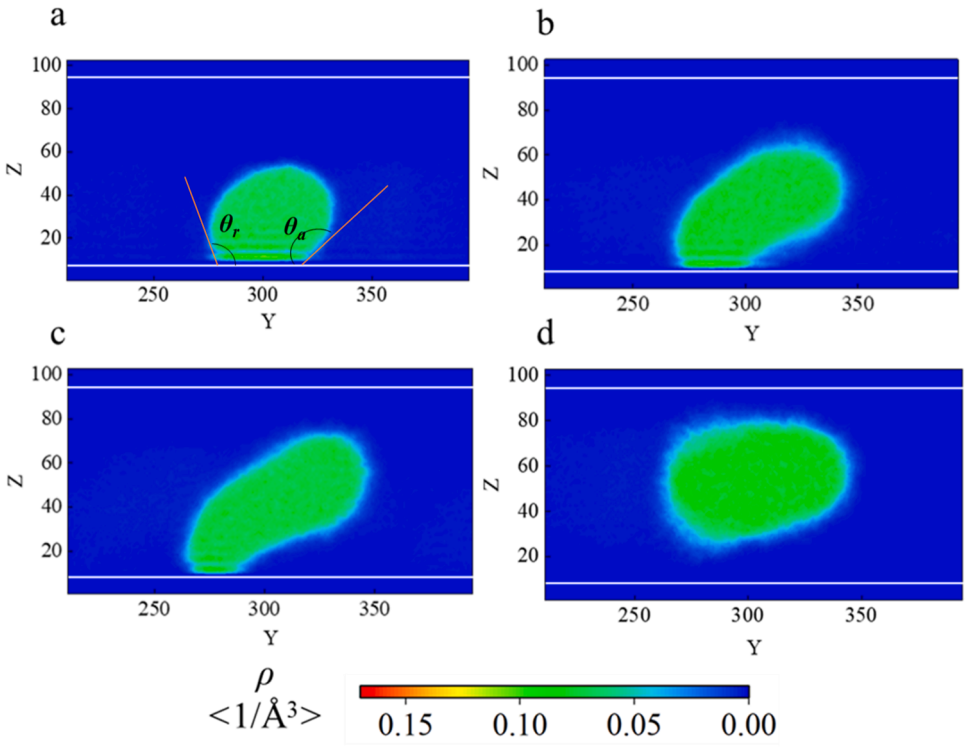

Fig. 16. Time-averaged oil/surfactant aggregate shape in NEMD simulation. Each panel is averaged over a time period of 5 ns. From a to d: the number of surfactant molecules: N = 0, 30, 45, 60. T = 330 K and P = 18.5 ± 0.6 MPa.

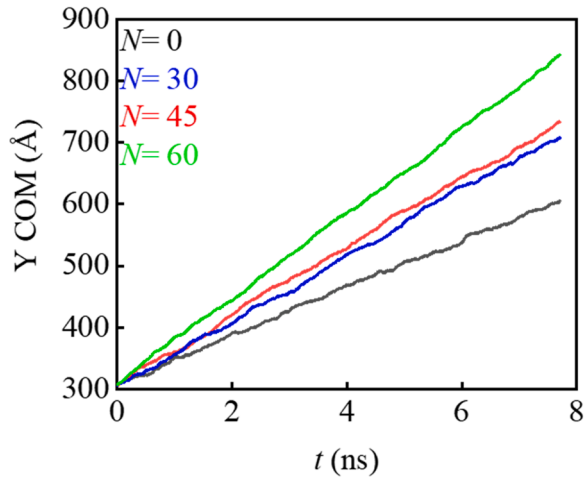

Fig. 17. A comparison of the change of the center of mass COM of the oil droplet along the water-flow direction under the SDBS surfactant flooding. External force F= 1.0×10^{-4} Kcal/mol-Å, corresponding to 3×10^{8} MPa/m. $T = 330$ K and $P = 18.5 \pm 0.6$ MPa.

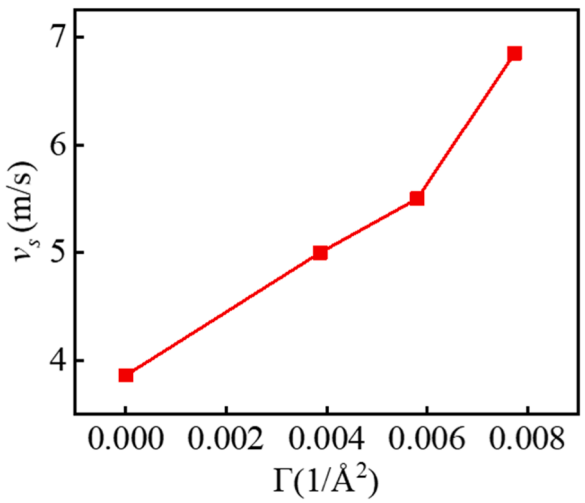

Fig. 18. Oil/surfactant aggregate displacement speed as a function of surface surfactant concentration. System conditions are the same as in Fig. 17.

averaging process, we move with the sliding drop. It is shown that an increased number of surfactant molecules absorbed at oil/water interface (surface concentration) leads to a strong oil droplet deformation. To characterize the deformation, an advancing (θ_a) and receding contact angle (θ_r) has been defined. They are determined by fitting two circular arcs to the time-averaged outline of the yz midplane of a droplet, one at the advancing side and one at the receding side of the drop, see our previous work [43]. It has to be noted that only in water flooding simulation, see Fig. 16 (a), both advancing and receding contact angle can be well estimated of the value of 124° ± 3.2° and 138° ± 2.8°, compared to its static contact angle of 132.4° ± 3.4°. However, for surfactant flooding where the advancing side of the droplet has a complex shape with, for example in Fig. 16 (b) and (c), curvature changing sign, θ_a could not be determined, that is something earlier reported in Derksen's work [8], and thus the contact angle is not discussed further. "Upon surfactant interactions, water molecules penetrate into the oil layer and propagate onto the rock surface" [36]. As a result, the rock surface occupied sites (previously by oil) are gradually replaced by water molecules after adding surfactant molecules. This finally leads to complete oil droplet detachment from the solid surface at $N = 60$, with corresponding $\Gamma = 0.008$ (1/Å^2). Where droplet completely lifts off the solid surface in the EMD simulation (see Fig. 13 **d**), the oil/surfactant aggregate has relatively small deformation (Fig. 16 **d**).

The effect of surfactant flooding on oil droplet displacement is represented again by tracking the centre of mass of the oil droplet as a function of time, see Fig. 17. Surfactant additions have a positive effect on the oil displacement, and the displacement speed is dependent on the surfactant surface concentration. Where the complete detachment oil ($N = 60$) under surfactant flooding sees the highest oil displacement speed, the speed is about 1.8 times higher than that in the identical pressure driven water flooding (slope of straight fits to green data and black data is 68 and 38 Å/ns respectively). The simulated results indicate surfactant additions result in change in oil contact angle (rock surface wettability) as a result of strong interactions between water/surfactant and oil/surfactant. The strong water wetting system further increases the oil displacement efficiency under surfactant flooding. The displacement speeds v_s as a function of surface surfactant concentration Γ is shown in Fig. 18.

4. Conclusion

In this work, we have presented a full-atoms MD study to investigate the oil droplet displacement in the silica nano-slit under surfactant flooding. In the first place, the behavior of the micellization of surfactant molecules in aqueous solution has been validated. In the second place the surfactant impact on significant IFT reduction for oil/water system is studied and such reduction is dependent on surfactant surface concentration. Finally, the oil droplet transport in nano slit under surfactant flooding is investigated. The main conclusions of our simulation are:

- Close with literature results, a radius of 22.85 Å micelle is formed by 60 SDBS surfactant molecules in aqueous solution at $T = 300$ K and $P = 1$ atm.
- The fundamental mechanism of IFT reduction with surfactant additions is described from a microscopic perspective. Interfacial thickness has a increase from 3.5 Å to 22.5 Å for the oil/water system at $T = 300$ K and $P = 1$ atm after surfactant molecules are absorbed at oil/water interface; the calculated interface formation energy of a single surfactant molecule is −145.7 Kcal/mol, indicating a decrease of system energy with surfactant additions as a result of a strong interaction between surfactant/dodecane and surfactant/water.
- For water flooding, the oil displacement speed is proportional to the external force F mimicking the pressure gradient. Compared to water flooding, surfactant additions would strongly change the rock surface wettability – oil droplet contact angle increases with surfactant additions until it completely detaches from substrate at surfactant surface concentration equals to 0.008 1/Å^2– and displace oil that was previously adsorbed at pore surface.
- Under an identical pressure gradient driven, the oil droplet deformation and displacement speed have a positive relation with its static contact angle (the larger the static contact angle, the stronger the droplet deformation and the higher the displacement speed). However, limited deformation is observed as oil droplet detaches from the solid substrate.
- Compared with water flooding, adding surfactant can significantly increase (up to 80 %) oil displacement speed. Where it has the highest displacement speed, oil drop completely lifts off solid substrate.

In the future we will be working on the effect of surfactant size, including molecule mass and its hydrocarbon chains lengths), and headgroups on interfacial properties to account for more complicated situations and investigate its effect on oil/water flow transport.

CRediT authorship contribution statement

Zhou Yingfang: Formal analysis, Funding acquisition, Investigation,

Project administration, Resources, Writing – review & editing. **Yong Wei:** Conceptualization, Data curation, Formal analysis, Investigation, Methodology, Validation, Visualization, Writing – original draft. **Wei Zhijie:** Investigation, Resources, Writing – review & editing.

Declaration of Competing Interest

The authors declare that they have no known competing financial interests or personal relationships that could have appeared to influence the work reported in this paper.

Data availability

Data will be made available on request.

Acknowledgments

This work was supported by National Natural Science Foundation of China (52074347).

References

[1] Accelrys Materials Studio, 2016. ⟨http://accelrys.com/products/collaborative-science/biovia-materials-studio/⟩.
[2] W.G. Anderson, Wettability literature survey part 5: the effects of wettability on relative permeability, J. Pet. Technol. 39 (1987), 1,453-1,468.
[3] J.L. Chen, B. Xue, D.B. Harwood, Q.P. Chen, C.J. Peters, J.I. Siepmann, A Monte Carlo simulation study of the interfacial tension for water/oil mixtures at elevated temperatures and pressures: Water/n-dodecane, water/toluene, and water/(n-dodecane toluene), Fluid Phase Equilibria 476 (2018) 16–24.
[4] Y. Chen, G. Xu, S. Yuan, H. Sun, Molecular dynamics simulations of AOT at isooctane/water interface, Colloids Surf. A: Physicochem. Eng. Asp. 273 (2006) 174–178.
[5] Y. Croonen, E. Gelad, M. Van der Zegel, M. Van der Auweraer, H. Vandendriessche, F.C. De Schryver, M. Almgrent, Influence of salt, detergent concentration, and temperature on the fluorescence quenching of 1-methylpyrene in sodium dodecyl sulfate with m-dicyanobenzene, J. Phys. Chem. 87 (1983) 1426–1431.
[6] T. Darden, D. York, L. Pedersen, Particle mesh Ewald: An N· log (N) method for Ewald sums in large systems, J. Chem. Phys. 98 (1993) 10089–10092.
[7] A. Das, S.M. Ali, Understanding of interfacial tension and interface thickness of liquid/liquid interface at a finite concentration of alkyl phosphate by molecular dynamics simulation, J. Mol. Liq. 277 (2019) 217–232.
[8] J.J. Derksen, Droplets sliding over shearing surfaces studied by molecular dynamics, AIChE J. 61 (2015) 4020–4027.
[9] T. Dong, N.B. Harris, 2013. 8 Pore Size Distribution and Morphology in the Horn River Shale, Middle and Upper Devonian, Northeastern British Columbia, Canada.
[10] T. Fang, Y. Zhang, R. Ma, Y. Yan, C. Dai, J. Zhang, Oil extraction mechanism in CO_2 flooding from rough surface: Molecular dynamics simulation, Appl. Surf. Sci. 494 (2019) 80–86.
[11] J. Gan, D. Wang, Z. Xiao, Y. Wang, K. Zhang, X. Zhu, S. Li, Experimental and molecular dynamics investigations of the effects of ionic surfactants on the wettability of low-rank coal, Energy 271 (2023) 127012.
[12] S.G. Grubb, M.W. Kim, T. Rasing, Y.R. Shen, Orientation of molecular monolayers at the liquid-liquid interface as studied by optical second harmonic generation, Langmuir 4 (1988) 452–454.
[13] J. He, Y. Ju, K. Kulasinski, L. Zheng, L. Lammers, Molecular dynamics simulation of methane transport in confined organic nanopores with high relative roughness, J. Nat. Gas. Sci. Eng. 62 (2019) 202–213.
[14] S. Iglauer, M.S. Mathew, F. Bresme, Molecular dynamics computations of brine–CO_2 interfacial tensions and brine–CO_2–quartz contact angles and their effects on structural and residual trapping mechanisms in carbon geo-sequestration, J. Colloid Interface Sci. 386 (2012) 405–414.
[15] R. Itri, L.Q. Amaral, Distance distribution function of sodium dodecyl sulfate micelles by x-ray scattering, J. Phys. Chem. 95 (1991) 423–427.
[16] S.S. Jang, S. Lin, P.K. Maiti, M. Blanco, W.A. Goddard, P. Shuler, Y. Tang, Molecular dynamics study of a surfactant-mediated decane− water interface: Effect of molecular architecture of alkyl benzene sulfonate, J. Phys. Chem. B 108 (2004) 12130–12140.
[17] M.M. Knock, G.R. Bell, E.K. Hill, H.J. Turner, C.D. Bain, Sum-frequency spectroscopy of surfactant monolayers at the oil− water interface, J. Phys. Chem. B 107 (2003) 10801–10814.
[18] C.M. Koretsky, D.A. Sverjensky, N. Sahai, A model of surface site types on oxide and silicate minerals based on crystal chemistry; implications for site types and densities, multi-site adsorption, surface infrared spectroscopy, and dissolution kinetics, Am. J. Sci. 298 (1998) 349–438.
[19] J. Li, Y. Han, G. Qu, J. Cheng, C. Xue, X. Gao, T. Sun, W. Ding, Molecular dynamics simulation of the aggregation behavior of N-Dodecyl-N,N-Dimethyl-3-Ammonio-1-Propanesulfonate/sodium dodecyl benzene sulfonate surfactant mixed system at oil/water interface, Colloids Surf. A: Physicochem. Eng. Asp. 531 (2017) 73–80.
[20] X. Liu, Y. Kang, L. Yan, J. Tian, J. Li, L. You, Implication of interfacial tension reduction and wettability alteration by surfactant on enhanced oil recovery in tight oil reservoirs, Energy Rep. 8 (2022) 13672–13681.
[21] Q. Liu, S. Yuan, H. Yan, X. Zhao, Mechanism of oil detachment from a silica surface in aqueous surfactant solutions: molecular dynamics simulations, J. Phys. Chem. B 116 (2012) 2867–2875.
[22] Q. Liu, X. Zhang, Q. Zhang, T. Wang, B. Jiang, Molecular dynamics simulations of dodecane detachment from hydrophobic SiO_2 in CTAB solutions, Colloids Surf. A: Physicochem. Eng. Asp. 653 (2022) 130020.
[23] D.M. Mitrinović, A.M. Tikhonov, M. Li, Z. Huang, M.L. Schlossman, Noncapillary-wave structure at the water-alkane interface, Phys. Rev. Lett. 85 (2000) 582.
[24] I. Ngo, F. Srisuriyachai, K. Sasaki, Y. Sugai, R. Nguele, Effects of reversibility on enhanced oil recovery using sodium dodecylbenzene sulfonate (SDBS), J. Jpn. Pet. Inst. 64 (2019) 188–198.
[25] T.X.D. Nguyen, S. Razavi, D.V. Papavassiliou, Janus nanoparticle and surfactant effects on oil drop migration in water under shear, J. Phys. Chem. B (33) (2022) 6314–6323.
[26] F. Palazzesi, M. Calvaresi, F. Zerbetto, A molecular dynamics investigation of structure and dynamics of SDS and SDBS micelles, Soft Matter 7 (2011) 9148–9156.
[27] F. Pan, Z. Zhang, X. Zhang, A. Davarpanah, Impact of anionic and cationic surfactants interfacial tension on the oil recovery enhancement, Powder Technol. 373 (2020) 93–98.
[28] S. Plimpton, Fast parallel algorithms for short-range molecular dynamics, J. Comput. Phys. 117 (1995) 1–19.
[29] M.J. Rosen, J.T. Kunjappu, Surfactants and interfacial phenomena, John Wiley & Sons, 2012.
[30] M. Sedghi, M. Piri, L. Goual, Molecular dynamics of wetting layer formation and forced water invasion in angular nanopores with mixed wettability, J. Chem. Phys. 141 (2014) 194703.
[31] Shen, V.K., Siderius, D., Krekelberg, W.P., Hatch, H.W., 2011. NIST Standard Reference Simulation Website, NIST Standard Reference Database Number 173. National Institute of Standards and Technology, Gaithersburg MD.
[32] M.R. Stukan, P. Ligneul, J.P. Crawshaw, E.S. Boek, Spontaneous imbibition in nanopores of different roughness and wettability, Langmuir 26 (2010) 13342–13352.
[33] H. Sun, S.J. Mumby, J.R. Maple, A.T. Hagler, An ab initio CFF93 all-atom force field for polycarbonates, J. Am. Chem. Soc. 116 (1994) 2978–2987.
[34] X. Sun, J. Liu, X. Dai, X. Wang, L.M. Yapanto, A.O. Zekiy, On the application of surfactant and water alternating gas (SAG/WAG) injection to improve oil recovery in tight reservoirs, Energy Rep. 7 (2021) 2452–2459.
[35] S. Supple, N. Quirke, Molecular dynamics of transient oil flows in nanopores I: Imbibition speeds for single wall carbon nanotubes, J. Chem. Phys. 121 (2004) 8571–8579.
[36] X. Tang, S. Xiao, Q. Lei, L. Yuan, B. Peng, L. He, J. Luo, Y. Pei, Molecular dynamics simulation of surfactant flooding driven oil-detachment in nano-silica channels, J. Phys. Chem. B 123 (2019) 277–288.
[37] M. Waldman, A.T. Hagler, New combining rules for rare gas van der Waals parameters, J. Comput. Chem. 14 (1993) 1077–1084.
[38] Y. Xiong, T. Cao, Q. Chen, Z. Li, Y. Yang, S. Xu, S. Yuan, J. Sjöblom, Z. Xu, Adsorption of a polyaromatic compound on silica surfaces from organic solvents studied by molecular dynamics simulation and AFM imaging, J. Phys. Chem. C. 121 (2017) 5020–5028.
[39] J. Xu, Y. Zhang, H. Chen, P. Wang, Z. Xie, Y. Yao, Y. Yan, J. Zhang, Effect of surfactant headgroups on the oil/water interface: An interfacial tension measurement and simulation study, J. Mol. Struct. 1052 (2013) 50–56.
[40] Y. Xu, Y. Liu, G. Liu, Molecular dynamics simulation of primary ammonium ions with different alkyl chains on the muscovite (001) surface, Int. J. Miner. Process. 145 (2015) 48–56.
[41] Y. Yan, C. Li, Z. Dong, T. Fang, B. Sun, J. Zhang, Enhanced oil recovery mechanism of CO_2 water-alternating-gas injection in silica nanochannel, Fuel 190 (2017) 253–259.
[42] W. Yong, J. Derksen, Y. Zhou, The influence of CO_2 and CH4 mixture on water wettability in organic rich shale nanopore, J. Nat. Gas. Sci. Eng. 87 (2020) 103746.
[43] W. Yong, Y. Zhou, A molecular dynamics investigation on methane flow and water droplets sliding in organic shale pores with nano-structured roughness, Transp. Porous Media (2021).
[44] S. Zeppieri, J. Rodríguez, A.L. López de Ramos, Interfacial tension of alkane water systems, J. Chem. Eng. Data 46 (2001) 1086–1088.
[45] Z.H. Zhang, I. Tsuyumoto, T. Kitamori, T. Sawada, Observation of the dynamic and collective behavior of surfactant molecules at a water/nitrobenzene interface by a time-resolved quasi-elastic laser-scattering method, J. Phys. Chem. B 102 (1998) 10284–10287.
[46] Y. Zhou, J. Helland, D.G. Hatzignatiou, A dimensionless capillary pressure function for imbibition derived from pore-scale modeling in mixed-wet-rock images, SPE J. 18 (2012) 296–308.